Eur. J. Mineral.
2002, **14**, 795–807

This paper was presented at the EMPG VIII
meeting in Bergamo, Italy (April 2000)

Fayalite and kirschsteinite solid solutions in melts from burned spoil-heaps, South Urals, Russia

ELLA SOKOL[1]*, VICTOR SHARYGIN[1], VALERY KALUGIN[2], NINA VOLKOVA[1] and ELENA NIGMATULINA[2]

[1]Institute of Mineralogy and Petrography of Russian Academy of Science,
[2]Institute of Geology of Russian Academy of Science,
Koptyuga prospect 3, 630090 Novosibirsk, Russia
* Corresponding author, e-mail: sokol@uiggm.nsc.ru or nvolkova@uiggm.nsc.ru

Abstract: Individual grains of calcian fayalite and ferroan kirschsteinite, as well as fayalite-kirschsteinite intergrowths are observed in the groundmass of basic crystallised melts, or *parabasalts*, from burned spoil-heaps of the Chelyabinsk brown-coal basin. Exsolved fayalite and kirschsteinite rims surround the grains of fayalite and early Mg-Fe olivine. The chemical study of the olivines has shown that during their crystallisation they were becoming enriched in fayalite and larnite and depleted in forsterite. The intergrowths of ferroan kirschsteinite (> 20 wt.% of CaO) and calcian fayalite (< 8.5 wt.% of CaO) are the exsolution products of an initially homogeneous Ca-Fe olivine with CaO > 8.5 wt.%. The exsolution temperatures were estimated to 980-800 °C. The main reasons for the appearance of the Ca-Fe olivine in the parabasalts are the composition of the initial melt enriched in FeO and CaO, fractional crystallisation resulting in further enrichment in iron of the residual low-silica melt, and reducing conditions during olivine crystallisation and exsolution.

Key-words: Ca-Fe olivine, fayalite, kirschsteinite, exsolution, burned spoil-heap.

Introduction

The CaO abundance in plutonic olivines does not usually exceed more than 1–2 wt. % (Simkin & Smith, 1970; Stormer, 1973; Deer *et al*., 1982). However, olivines crystallised from strongly silica-undersaturated magmas are occasionally rich in $CaFeSiO_4$ and/or $CaMgSiO_4$. In general, the predominance of Mg over Fe^{2+} leads to crystallisation of monticellite rather than to kirschsteinite. Kirschsteinite is a rarity in nature and is known to be produced in only a few terrestrial occurrences. The Mg-rich kirschsteinite has been found in melilite nephelinites from Mt. Shaheru, Zaire (Sahama & Hytönen, 1957), carbonatites from the Kuznetsk Alatau, Russia (Tolstykh *et al*., 1991), flood-basalts from the Dzhaltul Massif, Russia (Oleinikov, 1995), and kimberlites from Kotakonda, India (Chalapathi *et al*., 1996). At the same time, olivine of the $Ca(Fe,Mg)SiO_4$–$(Fe,Mg)_2SiO_4$ series is relatively common in different extraterrestrial materials: angritic achondrites (Prinz *et al*., 1977; Mittlefehldt & Lindstrom, 1990; Mikouchi *et al*., 1995; McKay *et al*., 1998; Longhi, 1999), chondrites (Dodd, 1971; Krot *et al*., 2000) and iron meteorites (Folco & Mellini, 1997).

Experimental and petrological data suggest that crystallisation of kirschsteinite is possible only from Ca-Fe-rich silica-undersaturated melts under reducing low-pressure conditions (Gustafson, 1972; Prinz *et al*., 1977; Longhi, 1999). Such a combination of chemical and physical factors occurs rarely in nature, which explains the lack of olivines of the Fe_2SiO_4–$CaFeSiO_4$ series. However, these minerals are the natural counterpart of high-temperature synthetic phases common in iron sinters (Wyderko & Mazanek, 1968) and also are found in the debris associated with underground nuclear explosion (Kahn & Smith, 1966). Glasses similar in composition to $CaFeSiO_4$ are present in coal fly ashes (Anshits *et al*., 1998).

The Fe-Mg mixing in the olivine solid solution can be considered to be nearly ideal and the Fe-Mg cation distribution in this mineral is almost completely disordered (Davidson & Mukhopadhyay, 1984). As a consequence, the Mg_2SiO_4–Fe_2SiO_4 series shows continuous solid solution at low pressures and temperatures. The solution properties of quadrilateral olivines in the system Mg_2SiO_4–Fe_2SiO_4–$CaMgSiO_4$–$CaFeSiO_4$ are radically different (Davidson & Mukhopadhyay, 1984). Complete partitioning of Ca on the M2 sites leads to limited miscibility between high-Ca and low-Ca olivines, which increases with increasing temperature and Fe content. Both the forsterite–monticellite and fayalite–kirschsteinite series exhibit continuous solid solution at high temperatures, but they show only limited miscibility across the solvus at low temperatures. Exsolution occurs when an originally homogeneous phase $(Fe,Mg,Ca)_2SiO_4$ enters a two phase field, usually as a result of cooling. As a consequence high-Ca olivine frequently forms lamellae in a matrix of low-Ca olivine. The exsolution phenomenon in

DOI: 10.1127/0935-1221/2002/0014-0795

0935-1221/02/0014-0795 $ 5.85

Ca-rich olivine is therefore a potential indicator of the cooling history of objects (Mikouchi *et al*., 1995; McKay *et al*., 1998; Markl *et al.*, 2001).

A basic melt-rock, or *parabasalt*, that occurs in the Chelyabinsk burned spoil-heaps (South Urals, Russia), contains abundant Fe_2SiO_4–$CaFeSiO_4$ olivines, which are the subject of this paper. Here the term "parabasalt" is used by analogy with the term "paralava", which is defined as a fusion product of sediments overlying and associated with naturally combusted coal seams (Fermor, 1918; Venkatesh, 1952; Cosca & Peacor, 1987; Cosca *et al*., 1989). It should be remarked that pyrometamorphic processes caused by coal fires in spoil-heaps give rise to man-induced rocks. According to the recommendations by IMA (Nickel & Grice, 1998), the constituents of these rocks cannot be considered as natural minerals, but only as their synthetic analogues. However, synthetic substances that correspond to existing minerals may be given mineral names if the synthetic origin of such substances is clearly stated (Nickel, 1995).

The purpose of this paper is to describe Ca-Fe olivines from the parabasalts, to reconstruct the bulk composition of initially homogeneous Fe_2SiO_4–$CaFeSiO_4$ solid solutions, and to discuss the possible conditions of Ca-Fe olivine crystallisation and following exsolution.

Analytical techniques

The major-element composition of parabasalt samples was determined by X-ray fluorescence method; FeO and Fe_2O_3, F, S, CO_2, H_2O^+, H_2O^- were determined by chemical method. Doubly-polished rock sections of about 50–100 μm in thickness have been used for optical microscopy in transmitted and reflected light. Thermometric investigations of silicate-melt inclusions hosted by parabasalt minerals were carried out with a high-temperature (>1300 °C) heating stage. Quantitative mineral analyses were performed using a CAMEBAX electron microprobe. An accelerating voltage of 20 kV and beam current of 10–20 nA was employed. A broad beam (10 μm diameter) was used for determination of average composition of Ca-Fe olivine intergrowths. Compositions of distinct phases (silicates, apatite, glasses and spinel) were determined for individuals of size more than 5 μm, as the minimum diameter of the beam was 2 μm. Concentrations were obtained with precision better than 1–2 % for the major elements, and 2–5 % for the minor elements. All analyses were carried out at the United Institute of Geology, Geophysics and Mineralogy, Novosibirsk, Russia. Back-scattered electron images (BSE) images were carried out with a LEO 420 electron scanning microscope at the Institute of Hydrodynamics, Novosibirsk, Russia.

Origin, mineralogy and petrography of parabasalts

The original waste material supplied to the spoil-heaps of the Chelyabinsk coal basin contains mudstones, siltstones, pieces of petrified wood (ankerite-dolomite), siderite concretions, and coal-bearing material. Spontaneous oxidation of the coal material in the heaps, with associated flame combustion took place between 1960 and 1980. At the present time the combustion of coal has been completed, and the heaps are composed of variably annealed and melted rocks. The dominant types of pyrometamorphic rocks – clinkers and different paralavas were studied earlier by Sokol *et al*. (1998, 2001, 2002) and Sharygin *et al*. (1999b).

Man-induced parabasalts are the products of the whole melting of waste material and subsequent melt crystallisation in hot spoil-heaps (Chesnokov & Shcherbakova, 1991; Sharygin *et al*., 1999b). The melt source was a finely crushed mixture of mudstones, calcareous clays, siderite concretions and carbonaceous material. The origin of highly ferrous melts through melting of a siderite-bearing substratum is identical for natural pyrometamorphic rocks from East Kazakhstan (Kalugin *et al*., 1991) and parabasalts (Sokol *et al*., 2001). During coal combustion, temperatures obtained were estimated to be 900–1250 °C. The first portions of melts appear to originate in places enriched in siderite, due to low-themperature dissociation of $Fe(CO_3)$. The temperature increase resulted in simultaneous melting of annealed pelitic rocks, Ca-Mg and Fe carbonates. As a result, the silicate basic melts produced are significantly rich in FeO.

Parabasalts were found only in the largest and intensively burning spoil-heaps. The spots of melt generation are spatially matched with a system of channels, where the incandescent gases circulated (Chesnokov & Shcherbakova, 1991). Separate portions of the melt flowed to the bottom in peculiar "chambers" of up to several cubic metres size, where they cooled down step-by-step and crystallised protected by the overlying cone of heated rocks. In the spoil-heaps three varieties of parabasalts were distinguished (Sokol *et al*., 1998; Sharygin *et al*., 1999b): a) monolithic blocks of massive parabasalts; b) stalactites of basic paralavas, similar to those found in partially fused sedimentary rocks produced by natural combustion of coal seam in Canadian Cordillera (Bustin & Mathew, 1982); c) parabasalt veins of up to 2 cm width.

The formation of veined parabasalts occurred in a spoil-heap of mine N 42 ($V = 920000\ m^3$; $h = 74$ m) and was connected with a zone of intense heating of a middle part of the spoil-heap. Numerous gas channels of 5 to 30 cm diameter are observed here. The circulation of incandescent gases ensured local heating of this part and caused a carbonate-clay substratum to melt. Such a phenomenon took place in pyrometamorphic rocks associated with naturally burned coal beds in Powder River Basin, Wyoming (Cosca *et al*., 1989).

All the parabasalt varieties contain fayalite (Sharygin *et al*., 1999b), but Ca-Fe olivines were identified only in 7 samples related to the veined variety (N 42-17/1-7). These stones are greyish-green-coloured, massive, holocrystalline**,** fine- and medium-grained with typical ophitic texture, akin to dolerite in their appearance. Volume proportion of interstitial high-silica glass in the stones does not exceed 2 %. Quenching mineral textures and skeletal crystals which are typical for glassy natural paralavas (Cosca *et al*., 1989), were not found here. Textural features of the studied parabasalts are greatly distinct from glassy porous slags, buchites and paralavas widespread in natural pyrometamorphic

Table 1. Whole-rock composition (in wt. %) of natural Fe-rich basic paralavas from different localities in comparison with parabasalts of the Chelyabinsk coal basin.

	1	2*	3	4	5*	6	7	8	9	10
SiO_2	48.95	47.24	46.98	41.63	53.92	45.65	44.06	43.32	50.07	37.78
TiO_2	0.60	0.80	0.86	0.69	0.80	1.07	0.93	0.73	0.94	0.94
Al_2O_3	11.31	20.46	25.86	13.63	16.61	17.91	17.26	16.29	18.88	14.46
Fe_2O_3	38.08	14.87	14.06	20.15	12.21	1.19	0.94	1.41	0.92	1.57
FeO	-	-	0.36	10.73	-	12.64	11.29	16.92	11.03	18.82
MnO	0.26	0.12	0.19	0.35	0.18	0.27	0.21	0.24	0.19	0.26
MgO	1.30	2.19	1.97	2.72	1.92	4.62	5.67	6.46	3.38	5.61
CaO	1.14	9.80	8.70	6.37	10.12	13.86	16.39	11.53	10.53	16.07
Na_2O	0.01	1.36	0.50	0.40	0.87	0.20	0.05	0.24	0.33	0.17
K_2O	1.61	1.32	0.52	1.15	2.02	1.37	1.48	0.77	2.09	1.46
P_2O_5	0.26	1.84	0.39	0.69	0.61	0.68	0.51	0.36	0.41	0.77
H_2O^+	-	-	0.50	-	-	-	-	0.50	-	-
H_2O^-	0.96	-	0.29	-	-	-	-	-	-	-
F	-	-	-	-	-	-	-	0.02	-	0.09
S	-	-	0.02	-	-	-	-	0.04	-	0.10
CO_2	-	-	0.03	-	-	-	-	0.45	-	0.62
LOI	-1.42	-	-	1.14	0.72	0.25	1.09	-	0.83	
Total	103.52	100.00	101.5	99.65	99.98	99.71	99.88	99.28	99.60	98.72

Note: 1 – *Powder River Basin paralava* (83EU-3B) includes fayalitic olivine, Al- and Fe^{3+}-rich clinopyroxene (esseneite), dorrite, melilite, Fe-rich cordierite, anorthite, SiO_2 polymorphs, mullite, K-Ba feldspar, spinel-magnetite-hercynite and hematite-ilmenite solid solutions, K-Al high-silica glass (Cosca *et al*., 1989).
2 – *Buffalo coal buchite* consists of esseneite, Al- and Fe^{3+}-rich melilite, aluminous magnesioferrite, anorthite, Al- and Mg-rich hematite, pseudobrookite, glass (Foit *et al.*, 1987).
3 – *British Columbia pseudovolcanic rock* from burned coal beds includes anorthite, cordierite, hematite, tridymite, cristobalite and glass (Church *et al*., 1979).
4–5 – *East Kazakhstan glassy basic ferrous paralavas.* The main minerals are magnetite, augite, hedenbergite, bytownite-anorthite, and hematite; the minor minerals are fayalitic olivine, tridymite, K-feldspar, cordierite and magnesioferrite (Kalugin *et al.*, 1991).
6–10 – *original data on the Uralian parabasalts:* 6–7 – *massive parabasalt* (KP, KP-5): anorthite, augite, Mg-Fe olivine, fayalite, K-Ba feldspar, leucite, Al-spinel, titanomagnetite, apatite, pyrrhotite, Fe-rich basic and K-Al high-silica glasses; 8–9 – *veined parabasalt* (42-17/1, 42-17/2): anorthite, augite, Mg-Fe olivine, fayalite, kirschsteinite, hedenbergite, K-Ba feldspar, leucite, Al-spinel, titanomagnetite, ilmenite, apatite, pyrrhotite, K-Al high-silica glass; 10 – *stalactitic parabasalt* (0107): anorthite, augite, fayalitic olivine, kirschsteinite, leucite, Al-spinel, titanomagnetite, apatite, pyrrhotite, Fe-rich basic glass.
*Owing to the highly oxidizing conditions under which these rocks formed, all Fe reported by Foit *et al*. (1987) and Kalugin *et al*. (1991) is given as Fe_2O_3.

rocks (Venkatesh, 1952; Bentor *et al*., 1981; Cosca & Peacor, 1987; Foit *et al*., 1987; Cosca *et al*., 1989).

The analysed parabasalts from the Uralian spoil-heaps are similar in chemical composition to natural highly ferrous basic paralavas (Table 1). All these rocks are distinct from natural basalts in slightly higher contents of Al_2O_3, and Fe_2O_3(tot) and significantly lower concentrations of MgO, Na_2O and H_2O. In contrast to the known paralavas (Church *et al*., 1979; Foit *et al*., 1987; Cosca *et al*., 1989; Kalugin *et al*., 1991), the studied parabasalts display marked enrichment in CaO and essential predominance of FeO over Fe_2O_3.

The detailed mineralogical and petrographical description of veined parabasalts was given by Sharygin *et al.* (1999a and b). The early mineral association (samples 42-17/1-7) composing up to 90 % of the rock volume is represented by anorthite, aluminous augite, olivine (Fo_{20-60}), leucite, Al-spinel, and Ti-magnetite. The mesostasis (10 vol. %) consists of fayalite, Ca-Fe olivine, kirschsteinite**,** aluminous hedenbergite, sulphide blebs (pyrrhotite ± pyrite ± chalcopyrite), Ti-magnetite, apatite, ilmenite, K-Ba feldspar and K-rich anorthite, as well as K-Al high-silica glass

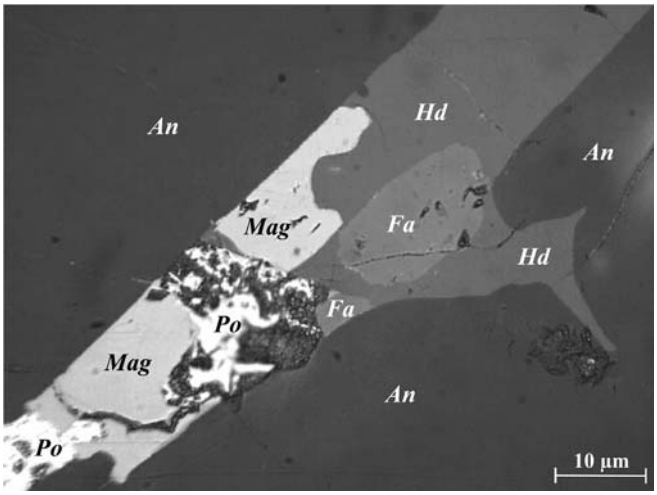

Fig. 1. General view showing interstitial association of veined parabasalt from the Chelyabinsk coal basin. Reflected light. Po – pyrrhotite, other mineral symbols as in Table 2.

(Fig. 1). Representative analyses of minerals and glass are given in Table 2.

Table 2. Representative analyses (wt. %) of minerals and interstitial glass from veined parabasalt, the Chelyabinsk coal basin.

	Early association						Late association							
Phase	Hc	An	Ol	Aug	Mag-1	Lct	Ap	Mag-2	Fa	Kir	Hd	Kfs	Ilm	Glass
SiO_2		44.46	35.91	45.17	0.14	55.49	5.51	0.17	30.22	32.24	45.81	57.74		77.21
TiO_2	0.26	0.00	0.03	1.43	10.17	0.01		22.05	0.00	0.02	0.02	0.19	47.35	0.40
Al_2O_3	57.62	34.67		12.85	3.49	22.71		1.50	0.00		3.74	19.91	0.22	11.76
Fe_2O_3	6.20			0.96	45.67	0.29		24.05			3.48	0.58	5.64	
Cr_2O_3	0.15			0.04	0.04			0.00					0.14	
V_2O_3	0.04												0.33	
FeO	24.43	0.84	36.26	3.97	37.93		1.54	50.71	60.84	35.93	23.09		44.01	1.53
MnO	0.31	0.03	0.62	0.09	0.02	0.01	0.04	0.71	2.19	0.85	0.97	0.01	0.53	0.03
MgO	10.66	0.06	25.49	11.10	1.73	0.02	0.24	0.23	1.72	3.99	0.35	0.02	1.74	0.06
CaO		19.36	1.41	24.44	0.12	0.01	53.92	0.02	4.79	26.39	22.26	0.69		0.99
Na_2O		0.27		0.03		0.23	0.11		0.04	0.05	0.34	0.08		0.13
K_2O		0.20				20.78						12.87		7.09
BaO		0.03				0.03						7.54		0.00
NiO	0.05		0.05		0.00			0.00					0.00	
ZnO	0.19				0.00			0.00					0.00	
P_2O_5							37.40		0.01	0.39				
SrO							0.20							
F							1.63							
Cl							0.24							0.02
Total	99.90	99.92	99.77	100.08	99.31	99.58	100.82	99.44	99.80	99.86	100.06	99.63	99.96	99.22
Anions	4	8	4	6	4	6		4	4	4	6	8	3	
Cations	3			4	3		10 #	3			4		2	
Si		2.066	1.010	1.668	0.005	2.018	0.921	0.006	1.000	0.989	1.869	2.820		
Ti	0.005	0.000	0.001	0.040	0.284	0.000		0.622	0.000	0.000	0.001	0.007	0.887	
Al	1.858	1.899		0.559	0.153	0.973		0.066	0.000		0.180	1.146	0.006	
Fe^{3+}	0.128			0.027	1.277	0.008		0.679			0.107	0.021	0.106	
Cr+V	0.004			0.001	0.001			0.000					0.009	
Fe^{2+}	0.559	0.033	0.853	0.123	1.179		0.215	1.590	1.683	0.922	0.788		0.916	
Mn	0.007	0.001	0.015	0.003	0.001	0.000	0.005	0.023	0.061	0.022	0.033	0.000	0.011	
Mg	0.435	0.004	1.069	0.611	0.096	0.001	0.061	0.013	0.085	0.182	0.021	0.002	0.065	
Ca+Sr		0.964	0.042	0.967	0.005	0.000	9.683	0.001	0.170	0.868	0.973	0.036		
Na		0.024		0.002		0.016	0.037		0.003	0.003	0.027	0.007		
K+Ba		0.013				0.964						0.946		
Ni+Zn	0.005				0.000			0.000					0.000	
P							5.292		0.000	0.010				
F+Cl							0.927							

Note: #-calculations on the basis of 10 cations in the Ca site. FeO and Fe_2O_3 were calculated from stoichiometry.
Mineral symbols: Hc = hercynite, An = anorthite, Ol = Mg-Fe olivine, Aug = augite, Mag = magnetite, Lct = leucite, Ap = apatite, Fa = fayalite, Kir = kirschsteinite, Hd = hedenbergite, Kfs = K-Ba feldspar, Ilm = ilmenite.

Silicate melt inclusions in minerals

Primary silicate melt inclusions (1–40 μm) have been studied in early minerals (anorthite, augite, Mg-Fe olivine, leucite, and apatite) of the veined parabasalts.

The growth zones of *anorthite* are decorated with melt inclusions and sometimes with Al-spinel crystals. The melt inclusions commonly consist of fine devitrified translucent Fe-rich glass ± shrinkage bubble ± sulphide globule ± daughter minerals (magnetite, augite, apatite, ferroan kirschsteinite, K-Ba feldspar or K-rich anorthite). Heating experiments with anorthite-hosted inclusions have shown that Fe-rich glass starts to fuse at 960–980 °C. The daughter K-Ba feldspar and K-rich anorthite disappear at 1060 and 1125 °C, respectively. Homogenisation temperatures of the inclusions range from 1170–1250 °C (central zones) to 1125–1140 °C (outer zones).

In *Mg-Fe olivine* the melt inclusions occur rarely in the central zones and are associated with anorthite and Al-spinel crystals. They consist of translucent devitrified glass ± shrinkage bubble or glass + shrinkage bubble ± sulphide globule ± daughter crystals (augite, magnesian kirschsteinite, Ti-magnetite, apatite). Some inclusions are composed only of crystalline phases (augite + kalsilite + magnetite +

Table 3. Representative analyses (wt. %) of glasses from silicate melt inclusions in minerals of veined parabasalt.

Host	An	An	An	An	Lct	Ol	Ol	Ap
Phase composition of inclusions	Gl_f+g	Gl_f+g	Gl_f+g	Gl_f	Gl_f+ Mag+g	Gl+Kir+ Ap+g	Gl+ Aug+g	Gl_f+g
T_{hom}, °C	1220	1185						
Phase	Gl_h	Gl_h	Gl_f	Gl_f	Gl_f	Gl	Gl	Gl_f
SiO_2	39.35	37.43	35.57	33.37	32.12	46.06	39.66	44.40
TiO_2	1.01	0.92	1.32	1.29	1.30	1.30	2.94	1.30
Al_2O_3	12.63	8.87	3.52	0.96	5.52	22.32	18.97	14.93
FeO	22.37	26.69	30.78	41.41	38.00	7.38	7.77	17.18
MnO	0.39	0.56	0.53	0.59	0.67	0.12	0.19	0.31
MgO	4.17	3.36	7.88	1.72	3.02	0.74	3.19	0.52
CaO	15.48	17.63	16.91	16.74	14.33	17.45	22.12	17.77
BaO	0.00	0.05	0.00	0.08	0.11	0.39	0.00	0.00
Na_2O	0.33	0.16	0.22	0.08	0.18	0.43	0.68	0.37
K_2O	2.16	1.35	1.47	0.02	0.25	2.91	2.24	1.29
P_2O_5	0.92	1.10	1.14	2.17	2.12	0.73	1.43	1.63
S	0.24	0.31	0.20	0.80	0.48	0.07	0.03	0.05
Total	99.02	98.44	99.54	99.22	98.11	99.90	99.22	99.75
Chemistry of host	$An_{97.5}$ $Ab_{2.2}$ $Or_{0.4}$	$An_{98.6}$ $Ab_{1.1}$ $Or_{0.3}$	$An_{98.2}$ $Ab_{1.5}$ $Or_{0.3}$	$An_{96.8}$ $Ab_{2.1}$ $Or_{1.1}$	$Lct_{98.6}$ $Anl_{1.4}$	$Fo_{57.5}$ $Fa_{40.0}$ $Ln_{2.5}$	$Fo_{57.5}$ $Fa_{40.0}$ $Ln_{2.5}$	oxy fluor apatite

Note: SrO, F, and Cr_2O_3 are below detection limit. Gl_f = Fe-rich devitrified glass; Gl = Ca-rich glass; Gl_h = heated glass; G = gas bubble; Ab = albite; Or = orthoclase; Anl = sodium leucite; Fo = forsterite; Ln = larnite, T_{hom} = homogenisation temperature of inclusions. Other symbols as in Table 2.

shrinkage bubbles). The glass-bearing inclusions have been heated only up to 1140 °C, because of abundant darkening of the host.

In *augite*, rare melt inclusions decorate the growth zones of the host. They consist of glass + shrinkage bubble + Ti-magnetite or fine devitrified glass + shrinkage bubble ± sulphide globule ± daughter minerals (hedenbergite, apatite, nepheline, Ti-magnetite). Homogenisation temperatures of the inclusions vary from 1200–1225 °C (central zones) to 1145–1175 °C (outer zones).

In *leucite* and *apatite* the melt inclusions were found in the central zones. They consist of fine devitrified opaque Fe-rich glass ± shrinkage bubble ± sulphide globule ± Ti-magnetite. Sometimes, completely crystallised inclusions (hedenbergite + kirschsteinite ± magnetite ± apatite + gas bubble) occur. Homogenisation temperatures of melt inclusions in leucite are higher than 1180 °C.

It should be noted that the homogenisation temperatures of the primary inclusions can be considered as minimum temperatures of host mineral formation. Thus, petrographic investigations and thermometry of the melt inclusions suggest that the paragenetic sequence of mineral formation in veined parabasalt was the following: Al-spinel → anorthite (1250–1125 °C) → Mg-Fe olivine (>>1140 °C) → augite (1225–1145 °C) → leucite (>1180 °C) → apatite, Ti-magnetite → K-rich anorthite (1125 °C), fayalite, kirschsteinite, hedenbergite → K-Ba feldspar (1060 °C). The melting temperatures of high-iron low-silica glass from the examined inclusions are estimated to be 960–980 °C and are coincident with those of K-Al high-silica interstitial glass.

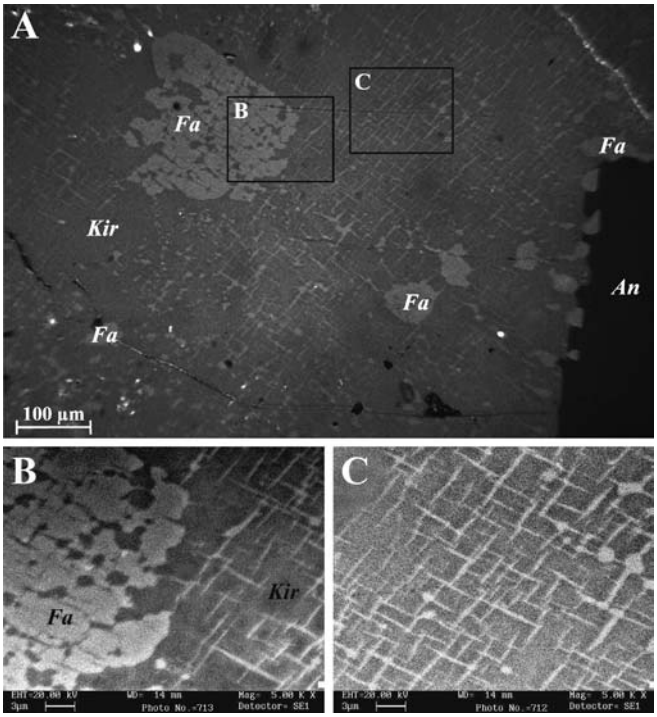

Fig. 2. Two kinds of exsolved textures for Ca-Fe olivine. A – general view of fayalite (Fa) and kirschsteinite (Kir) distribution, reflected light. B, C – BSE images of fayalite-kirschsteinite intergrowths; both lamellae and matrix may be represented by fayalite and kirschsteinite.

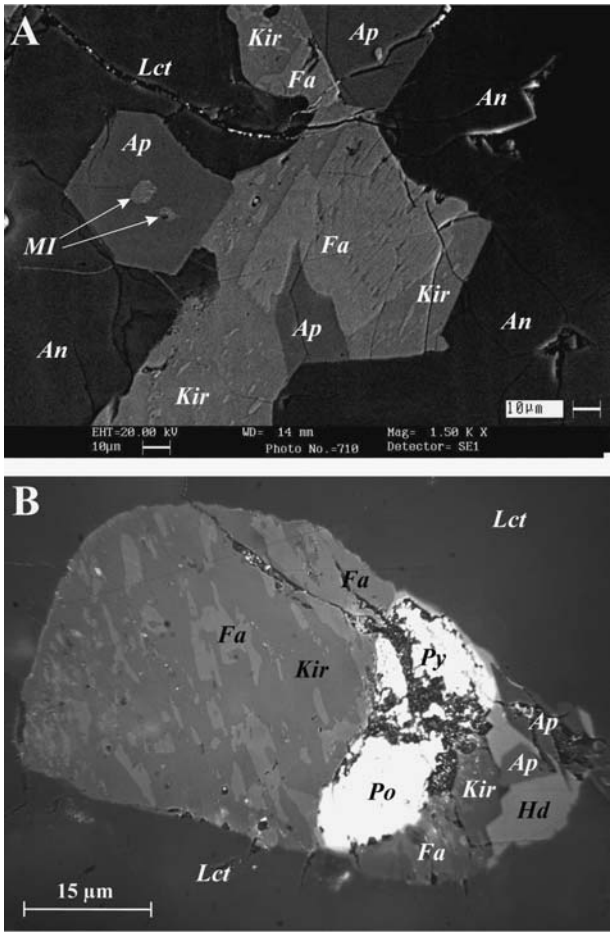

Fig. 3. Exsolved textures for fayalite-kirschsteinite intergrowths. BSE image (A) and optical micrograph in reflected light (B) of interstitial associations. Po – pyrrhotite, Py – pyrite, MI – melt inclusions in apatite, other mineral symbols as in Table 2.

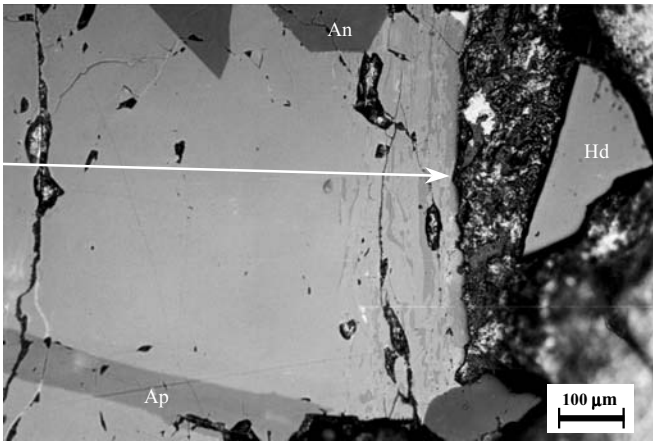

Fig. 4. A zoned Mg-Fe olivine–calcian fayalite grain with rim of kirschsteinite-fayalite intergrowths. Reflected light. Arrow shows microprobe profile (Table 4, grain B). Mineral symbols as in Table 2.

Electron microprobe analysis has shown that all the inclusion glasses in early minerals are essentially rich in CaO and FeO (Table 3). Devitrified glasses of plagioclase- and leucite-hosted inclusions are characterised by high FeO (22–41 wt. %), CaO (14–22 wt. %) and low SiO_2 (32–39 wt. %), Al_2O_3 (1–12 wt. %). The glasses of the inclusions from Mg-Fe olivine and apatite have higher SiO_2 (40–46 wt. %), Al_2O_3 (15–22 wt. %) and lower FeO (7–17 wt. %).

Morphological and chemical features of olivines from parabasalts

Early Mg-Fe olivine (Fo_{60-20}, CaO = 0.3–2.5 wt. %) in the veined parabasalt forms large (up to 0.5–1 mm) euhedral grains. Anhedral grains of calcian fayalite ($Fo_{9-8}Fa_{80-84}Tph_{2-3}Ln_{7-15}$, CaO = 4–8.5 wt. %) occur in the interstices.

Ca-Fe olivines mainly occur as varied fayalite-kirschsteinite intergrowths. Classical exsolution textures similar to those of Ca-rich olivines from the angrite LEW 86010 (Mikouchi *et al.*, 1995) are rare. They are represented by two sets of distinct thin lamellae (up to 0.2 µm), parallel to (031) and ($0\bar{3}1$) planes of the host olivine. Fayalite and kirschsteinite can form both lamellae and matrix (Fig. 2). Anhedral individuals being the intergrowths of calcian fayalite and kirschsteinite are the most common in the mesostasis (Fig. 3). Kirschsteinite occurs as abundant exsolved particles (0.1–2 µm) of irregular shape with subparallel orientation in the rims surrounding Mg-Fe olivine (Fig. 4) and fayalite, as well as in the zoned Ca-Fe olivines (Fig. 5A). Similar inclusions of magnesian kirschsteinite were observed in host Ca-rich olivine from the Sharps chondrite (Dodd, 1971) and from the Angra dos Reis achondrite (Prinz *et al.*, 1977). Subindividuals from the intergrowths under study usually are 0.1–2 µm wide, too small for individual microprobe analysis. Their uniform distribution permits reconstruction of the bulk composition of originally homogeneous Ca-Fe olivines by direct analysis of intergrowths using of broad beam of microprobe.

Representative microprobe traverses across crystals of Mg-Fe olivine bordered by rim of Ca-Fe olivine are shown in Fig. 6A, B. The rim thickness is 60–120 µm. Their cores display zonal patterns from Fo_{57} in the central parts up to Fo_{17} in the outermost parts of the cores. The bulk larnite (Ln) content in cores of these grains varies from 2 up to 8 mol. %. All the rims display sharp zoning, expressed in steep rise in Ca content and decrease in Fe content towards the outside of the grains. The content of MgO (< 2 wt. %) remains minimal (Table 4). The steep profiles and the ranges of the CaO and FeO concentrations are similar for all studied zoned individuals, including those having different mineral core compositions.

Analysis of the bulk composition of a zoned Ca-Fe olivine was carried out along the several linear profiles (Fig. 5B, Table 4). The mapping of the spatial distributions of the major end members in initial olivine (Fig. 5C, D) reveals high chemical gradients in CaO and FeO. The CaO content increases from the core (7–8.5 wt. %) to the rim (18–20 wt. %) with simultaneous decrease in the FeO content from 59 to 47 wt. %.

The various microstructures originated during cooling and exsolution of high-Ca olivine on a scale of a single grain (Fig. 5A). The core (Ln_{12-16}) appears to be homogeneous at

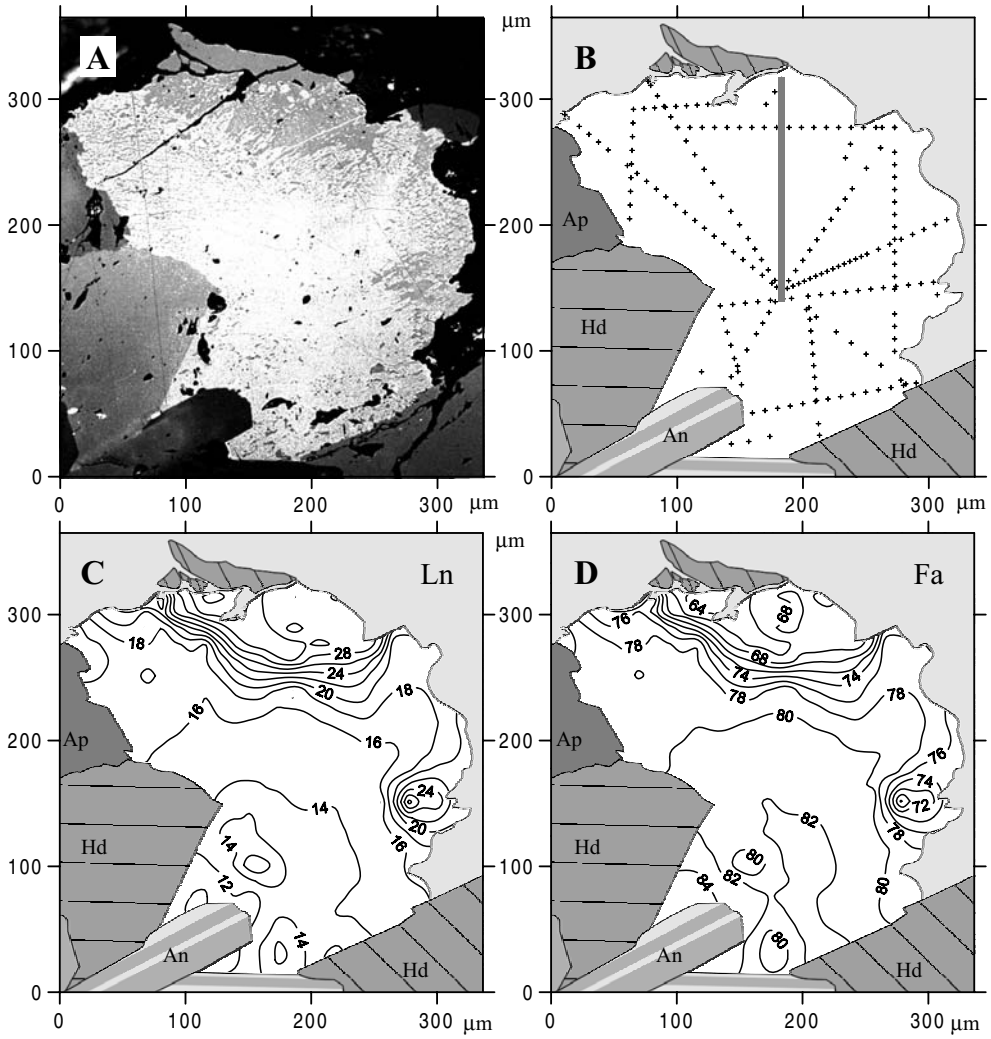

Fig. 5. Mapping of an originally homogeneous Ca-Fe olivine grain in terms of the end members.
A – image of the olivine grain, reflected light. B – map of microprobe analyses; crosses are analysed points; solid line is profile for the grain C in Table 4. C, D – maps in the concentrations of the larnite and fayalite end members, respectively. Mineral symbols as in Table 2.

magnification up to 1000×; it should be noted that this does not preclude the presence of crypto-exsolution textures. Kirschsteinite lamellae with minimum thickness < 0.2 µm can be observed in a zone, adjacent to the core (Ln_{16-18}). In the next zone with the bulk larnite content of 18–24 mol. %, exsolved lamellae are up to 2 µm in size. In the rim the concentration of CaO increases up to 15–20 wt. %. In this case Ca-Fe olivine (Ln_{26-34}) composes the matrix, while calcian fayalite (Ln_{12-18}) occurs as equant grains up to 10 µm in size. The large sizes of subindividuals can lead to errors in determination of the bulk compositions of the original Ca-Fe olivines when made in accordance with the above-mentioned procedure.

The compositions of the coexisting fayalite and kirschsteinite from the intergrowths were determined for subindividuals larger than 5 µm (Table 5). All fayalites, being the exsolution products, are calcian. Kirschsteinites have a low content of Mg and are ferroan. On the quadrilateral diagram the pairs of calcian fayalite and ferroan kirschsteinite plot close to the Fe_2SiO_4–$CaFeSiO_4$ side (Fig. 7). The pairs fit the miscibility gap surface (Davidson & Mukhopadhyay, 1984) well, suggesting that the fayalite-kirschsteinite intergrowths orginated due to the exsolution of Ca-Fe olivine.

Temperature and oxygen fugacity during crystallisation and exsolution of Ca-Fe olivines

The composition of zoned Ca-Fe olivines allows reconstruction of their crystallisation path, using the data from Mukhopadhyay & Lindsley (1983; Fig. 8). Calcian fayalite which are comparable in composition to Ca-Fe olivines from parabasalts (Ln_{7-30}) should crystallise on a narrow temperature range from 1150 to 1130 °C. Undoubtedly, the examined Ca-Fe olivines crystallised at somewhat lower temperature, as the diagram by Mukhopadhyay & Lindsley (1983) was constructed for the binary system Fe_2SiO_4–$CaFeSiO_4$ and does not take into account the presence of Mn, P, Ti, alkalis and other minor elements in the minerals and melts. As the olivines under consideration cooled below the temperature below fayalite-kirschsteinite solvus, they be-

Table 4. Representative analyses (wt. %) for profiles in zoned olivine grains in veined parabasalt.

Distance, μm	SiO_2	FeO	MnO	MgO	CaO	P_2O_5	Total	Fo	Fa	Tph	Ln
Grain A (zoned Mg-Fe olivine)											
0(C)	35.96	33.71	0.56	27.57	2.10	0.01	99.90	57.1	39.2	0.7	3.1
125	35.88	34.56	0.60	27.33	1.60	0.02	99.99	56.7	40.2	0.7	2.4
145	34.91	39.51	0.71	23.08	1.72	0.03	99.96	49.2	47.3	0.9	2.6
175	33.51	46.29	0.97	17.14	1.87	0.05	99.83	38.1	57.7	1.2	3.0
195	31.93	54.00	1.33	9.95	2.69	0.05	99.95	23.2	70.6	1.8	4.5
198	31.48	54.86	1.51	7.18	4.84	0.07	99.94	17.0	72.8	2.0	8.2
205	30.96	55.06	1.55	4.07	8.12	0.08	99.84	9.8	74.1	2.1	14.0
218	30.89	57.38	1.67	4.09	5.88	0.05	99.96	9.9	77.7	2.3	10.2
230	30.80	55.32	1.55	2.72	9.46	0.08	99.93	6.6	74.9	2.1	16.4
240	30.45	58.67	1.69	2.13	6.92	0.06	99.92	5.2	80.3	2.3	12.1
245	30.78	53.45	1.49	1.58	12.60	0.11	100.01	3.8	72.3	2.0	21.8
255	30.56	56.85	1.61	1.63	9.24	0.11	100.00	4.0	77.6	2.2	16.2
265(R)	31.13	47.59	1.31	1.11	18.70	0.13	99.97	2.6	63.6	1.8	32.0
Grain B (zoned Mg-Fe olivine – Ca fayalite)											
0(C)	34.79	40.47	0.69	22.60	1.41	0.00	99.97	48.4	48.6	0.8	2.2
110	32.98	49.31	1.06	14.47	2.21	0.01	100.04	32.6	62.4	1.4	3.6
195	31.60	55.90	1.48	7.88	3.25	0.04	100.15	18.6	73.9	2.0	5.5
300	30.73	59.05	1.76	3.86	4.60	0.06	100.06	9.3	80.2	2.4	8.0
355	30.47	59.47	1.86	2.57	5.48	0.06	99.91	6.3	81.5	2.6	9.6
425	30.37	59.68	1.83	1.80	6.18	0.04	99.90	4.4	82.1	2.6	10.9
440	30.34	59.34	1.85	1.45	6.90	0.06	99.94	3.6	81.7	2.6	12.2
450	30.41	58.22	1.87	1.27	8.15	0.06	99.98	3.1	80.0	2.6	14.3
457	30.18	61.25	1.84	1.22	5.42	0.01	99.92	3.0	84.8	2.6	9.6
462	30.38	58.35	1.77	1.55	7.76	0.06	99.87	3.8	80.1	2.5	13.6
480	30.30	59.53	1.84	1.47	6.74	0.06	99.94	3.6	81.9	2.6	11.9
490	30.35	58.41	1.85	1.11	8.16	0.10	99.98	2.7	80.3	2.6	14.4
500	30.41	57.83	1.80	1.07	8.79	0.06	99.96	2.6	79.4	2.5	15.5
510	30.13	61.59	1.92	1.10	5.20	0.01	99.95	2.7	85.4	2.7	9.2
520	30.75	52.28	1.63	0.81	14.31	0.09	99.87	2.0	70.9	2.2	24.9
530	30.70	53.62	1.61	0.82	13.11	0.07	99.93	2.0	72.9	2.2	22.8
540(R)	31.03	47.11	1.56	0.72	19.24	0.17	99.83	1.7	63.1	2.1	33.0
Grain C (originally homogeneous Ca-Fe olivine)											
0(C)	30.28	59.25	1.89	0.76	7.82	0.08	100.08	1.9	81.7	2.6	13.8
10	30.22	59.18	1.84	0.78	7.78	0.09	99.89	1.9	81.8	2.6	13.8
30	30.20	58.82	1.94	0.74	8.05	0.07	99.82	1.8	81.2	2.7	14.2
60	30.30	58.35	1.89	0.70	8.62	0.06	99.92	1.7	80.4	2.6	15.2
80	30.33	58.28	1.98	0.70	8.64	0.07	100.00	1.7	80.3	2.8	15.2
110	30.35	57.59	1.85	0.68	9.39	0.07	99.93	1.7	79.2	2.6	16.5
125	30.81	51.09	1.63	0.58	15.70	0.09	99.89	1.4	69.1	2.2	27.2
135	31.03	48.02	1.66	0.53	18.60	0.11	99.94	1.3	64.5	2.3	32.0
150	31.00	49.04	1.72	0.53	17.61	0.04	99.94	1.3	66.0	2.3	30.4
170	31.17	46.78	1.50	0.55	19.93	0.07	100.00	1.3	62.5	2.0	34.1
180	30.84	53.03	1.68	0.63	14.00	0.02	100.20	1.5	71.9	2.3	24.3
190(R)	31.05	49.50	1.44	0.67	17.28	0.03	99.97	1.6	66.6	2.0	29.8

Note: Microprobe beam diameter was 10 μm. C = core, R = rim. The distance is given from the core of the grains. Fo = forsterite, Fa = fayalite, Tph = tephroite, Ln = larnite. Complete profiles for grains A and B are shown in Fig. 6A and 6B, respectively. Photomicrographs of grains B and C are given in Fig. 4 and Fig. 5, accordingly.

gan to exsolve. The exsolved phases grew by diffusion and varied gradually in their composition as the mineral cooled and the solvus expanded (Fig. 8).

The olivine of the above-mentioned compositions should have undergone exsolution at T < 1030 °C. Plots of the coexisting fayalite-kirschsteinite pairs on the phase diagram (Davidson & Mukhopadhyay, 1984; Fig. 7) allow estimation of the temperature interval at the time of exsolution as $980 \le T \le 800$ °C. The temperature value of 800 °C may be interpreted as a minimum temperature of effective cation exchange.

The oxygen fugacity during the early stage of parabasalt crystallisation was calculated by the following regression equation:

$$\ln(X^{liq}_{Fe_2O_3} / X^{liq}_{FeO}) = a\ln f_{O_2} + b/T + c + \sum_i d_i X_i,$$

Table 5. Representative analyses of kirschsteinite-fayalite pairs from intergrowths.

	1		2		3		4		5		6		7		8	
	Fa	Kir	Fa	Kir	Fa	Kir	Fa	Kir	Fa	Kir	Fa	Kir	Fa	Kir	Fa	Kir
wt.%	N=2	N=4	N=2	N=1	N=1	N=1	N=1	N=1	N=1	N=2	N=1	N=2	N=1	N=1	N=1	N=2
P_2O_5	0.05	0.10	0.03	0.06	0.04	0.09	0.04	0.10	0.08	0.16	0.04	0.12	0.05	0.10	0.02	0.13
SiO_2	30.11	31.44	30.07	31.45	30.77	31.65	30.16	31.32	30.21	31.11	30.08	31.52	30.19	31.56	30.40	31.45
TiO_2	0.00	0.00	0.00	0.00	0.03	0.01	0.00	0.00	0.02	0.00	0.02	0.00	0.00	0.00	0.00	0.01
FeO	60.36	43.08	60.85	43.12	57.59	41.60	60.91	44.19	58.29	45.71	61.21	41.77	60.41	42.47	58.06	43.42
MnO	2.11	1.52	1.91	1.34	1.27	0.97	1.81	1.39	1.98	1.63	2.01	1.34	1.96	1.42	2.10	1.60
MgO	0.46	0.28	0.57	0.34	2.85	1.43	1.42	0.57	0.72	0.53	1.13	0.60	1.10	1.00	1.84	1.13
CaO	6.73	23.66	6.40	23.54	7.48	23.92	5.47	22.24	8.47	20.46	5.20	24.46	6.16	23.46	7.27	22.10
Na_2O	0.06	0.07	0.05	0.03	0.03	0.03	0.04	0.03	0.05	0.07	0.03	0.07	0.00	0.05	0.04	0.05
Total	99.88	100.14	99.87	99.88	100.06	99.71	99.85	99.84	99.81	99.65	99.72	99.88	99.87	100.06	99.73	99.88
Formula based on 4 oxygens																
P	0.001	0.003	0.001	0.002	0.001	0.002	0.001	0.003	0.002	0.004	0.001	0.003	0.001	0.003	0.001	0.003
Si	0.999	0.996	0.999	0.999	0.999	0.997	0.998	0.997	0.997	0.996	0.999	0.996	0.999	0.996	0.999	0.996
Ti	0.000	0.000	0.000	0.000	0.001	0.000	0.000	0.000	0.000	0.000	0.000	0.000	0.000	0.000	0.000	0.000
Fe	1.675	1.142	1.690	1.145	1.564	1.096	1.686	1.176	1.608	1.224	1.700	1.104	1.671	1.121	1.595	1.151
Mn	0.059	0.041	0.054	0.036	0.035	0.026	0.051	0.037	0.055	0.044	0.057	0.036	0.055	0.038	0.058	0.043
Mg	0.023	0.013	0.028	0.016	0.138	0.067	0.070	0.027	0.035	0.025	0.056	0.028	0.054	0.047	0.090	0.053
Ca	0.239	0.803	0.228	0.801	0.260	0.808	0.194	0.758	0.299	0.702	0.185	0.828	0.218	0.793	0.256	0.750
Na	0.004	0.004	0.003	0.002	0.002	0.002	0.003	0.002	0.003	0.004	0.002	0.004	0.000	0.003	0.003	0.003
M1+M2	2.000	2.003	2.002	2.000	1.999	2.000	2.003	2.001	2.002	1.999	2.000	2.001	1.999	2.003	2.002	2.000
Total	3.001	3.002	3.002	3.000	3.000	3.000	3.002	3.000	3.001	3.000	3.000	3.001	2.999	3.001	3.002	3.000
Mg#	1.3	1.1	1.6	1.3	7.9	5.6	3.9	2.2	2.1	2.0	3.1	2.4	3.1	3.9	5.2	4.3
End members of the olivine group																
Fo	1.1	0.7	1.4	0.8	6.9	3.4	3.5	1.3	1.8	1.3	2.8	1.4	2.7	2.3	4.5	2.7
Fa	83.7	57.0	84.4	57.3	78.2	54.8	84.2	58.8	80.4	61.2	85.0	55.2	83.6	56.0	79.7	57.5
Tph	3.0	2.0	2.7	1.8	1.7	1.3	2.5	1.9	2.8	2.2	2.8	1.8	2.8	1.9	2.9	2.1
Ln	12.2	40.3	11.5	40.2	13.1	40.5	9.8	38.0	15.1	35.3	9.4	41.6	10.9	39.8	12.9	37.7
End members of the monticellite group																
Mtc		1.1		1.3		5.4		2.0		1.8		2.3		3.7		4.0
Kir		76.3		76.1		73.5		71.1		65.7		77.9		72.8		68.1
Glc		3.3		2.9		2.1		2.8		3.1		3.0		3.0		3.2
Fa		19.4		19.7		19.0		24.0		29.4		16.8		20.5		24.7

Note: Microprobe beam diameter was 2 μm. 1–3 – intergrowths from originally homogeneous Ca-Fe olivine grains; 4–8 – intergrowths from rim around fayalite and Mg-Fe olivine grains. Mg# = 100 Mg/(Fe+Mg+Mn). N – number of analyses; Mtc = monticellite, Kir = kirschsteinite, Glc = glaucochroite, other abbreviations as in Table 4.

where X_i is the mole fraction of *i*-component in rock; *T* is temperature (*K*); *a, b, c* and d_i are regression coefficients (Kilinc *et al.*, 1983). Whole-rock compositions of the parabasalts (Table 1) are taken as melt compositions. The liquidus temperature of these melts were calculated according to the algorithm realised in the programme package COMAGMAT 3.0 (Ariskin *et al.*, 1993). It was established that in all examined cases the liquidus phase is anorthite (Table 6), which is confirmed by petrographic observations. It should be noted that Al-spinel is not considered in this algorithm. At the early stage of the Uralian parabasalts crystallisation, the f_{O2} was estimated to be $10^{-8.5} – 10^{-9.6}$ bar, which is 1 to 2 log units below the QFM buffer.

To estimate f_{O2} and a_{SiO2} during late crystallisation of parabasalt melt the QUILF program was used (Andersen *et al.*, 1993). For this purpose we analysed minerals from interstitial associations which usually contain homogeneous fayalite or kirschsteinite or exsolved Ca-Fe olivine (fayalite-kirschsteinite intergrowths), hedenbergite, magnetite, apatite and sulphides (Table 7, Fig. 1, 3B). The calculations were performed for the 1050–1100 °C range in which Ca-Fe olivine was homogenous according to the diagram of Mukhopadhyay & Lindsley (1983) (Fig. 8). When either magnetic or hedenbergite is absent in examined mineral assemblage, the average compositions of magnetite $Mag_{90}Usp_{10}$ and hedenbergite $En_3Fs_{50}Wo_{47}$ were used for calculations. The composition of initial Ca-Fe olivine is determined from modal proportions of fayalite and kirschsteinite in their intergrowths. According to the obtained results (Table 7), oxygen fugacities during crystallisation of parabasalt were

Table 6. The f_{O2} estimates at 1 bar and liquidus temperatures for parabasalt melts.

Sample	T_{liq} (°C)	Liq. phase	lg f_{O2}	ΔQFM
KP	1280	An_{99}	-8.56	-1.1
KP-5	1298	An_{100}	-8.75	-1.5
42-17/1	1198	An_{98}	-9.65	-1.3
42-17/2	1268	An_{98}	-8.75	-1.2
O107	1259	An_{99}	-9.48	-1.8

An = anorthite

Table 7. Chemical compositions (wt. %) and f_{O2}-a_{SiO2} estimations at T = 1050, 1100 °C and 1 bar of late mineral associations from veined parabasalt.

	Association	Mineral	SiO_2	TiO_2	Al_2O_3	FeO	MnO	MgO	CaO	Na_2O	Total	T,°C	lg f_{O2}	ΔQFM	a_{SiO2}
1	Fa_{50} + Kir_{50} + Hd	Fa	30.64	0.00	0.00	57.69	1.40	2.61	7.54	0.00	99.88	1100	-10.3	-0.8	0.44
		Kir	31.70	0.00	0.00	44.33	1.13	1.92	20.99	0.00	100.07	1050	-11.1	-0.9	0.40
		Hd	43.20	0.56	5.95	24.35	0.32	2.26	22.89	0.18	99.71				
2	Fa + Hd + Mag	Fa	30.57	0.00	0.00	59.63	1.57	2.55	5.62	0.00	99.94				
		Hd	43.69	0.54	5.84	24.10	0.31	2.82	22.74	0.13	100.17	1100	-10.2	-0.6	0.51
		Mag	0.28	2.59	5.82	84.43	0.24	0.16	0.30	0.00	93.82				
3	Fa_{50} + Kir_{50} + Ap +	Fa	30.70	0.00	0.00	59.31	1.48	3.19	5.41	0.00	100.09				
	Hd + Mag + Sulph	Kir	31.83	0.00	0.00	41.96	1.05	1.73	23.36	0.00	99.93	1100	-10.3	-0.7	0.43
		Hd	43.90	0.62	5.28	23.21	0.30	3.28	22.98	0.06	99.63				
		Mag	0.27	2.58	6.83	85.00	0.10	0.55	0.26	0.00	95.59				
4	Fa + Hd + Mag	Fa	29.99	0.00	0.00	62.86	2.52	1.12	3.51	0.00	100.00	1100	-10.2	-0.7	0.66
		Hd	42.69	0.84	5.56	26.92	0.39	0.97	22.16	0.10	99.63	1050	-11.0	-0.8	0.60
		Mag	0.24	7.25	4.26	82.64	0.52	0.14	0.26	0.00	95.31				
5	Fa_{40} + Kir_{60} +	Fa	30.01	0.00	0.00	62.71	1.62	0.67	4.88	0.00	99.89	1100	-10.3	-0.8	0.48
	Hd + Sulph	Kir	31.50	0.00	0.00	42.82	1.17	0.40	23.92	0.00	99.81	1050	-11.1	-0.9	0.45
		Hd	44.35	0.26	4.49	25.23	0.48	2.56	22.28	0.10	99.75				
6	Fa + Hd +	Fa	30.59	0.00	0.00	58.58	1.52	2.79	6.65	0.00	100.13				
	Mag + Sulph	Hd	43.51	0.61	5.40	24.28	0.33	2.59	22.59	0.17	99.48	1100	-10.3	-0.8	0.47
		Mag	0.34	2.49	6.57	84.20	0.35	0.30	0.35	0.00	94.60				
7	Fa_{30} + Kir_{70} + Ap +	Fa	30.07	0.00	0.00	60.98	2.02	0.53	6.25	0.00	99.85	1100	-10.3	-0.8	0.47
	Hd + Sulph	Kir	31.49	0.00	0.00	43.58	1.29	0.39	23.19	0.00	99.94	1050	-11.1	-0.9	0.45
		Hd	43.61	0.35	5.50	26.13	0.48	1.35	22.30	0.12	99.84				
8	Kir + Hd +Ap	Kir	31.51	0.00	0.00	42.19	1.24	0.35	24.57	0.00	99.86	1100	-10.0	-0.5	0.47
		Hd	44.67	0.03	4.11	27.17	1.03	0.43	22.00	0.15	99.59	1050	-10.8	-0.5	0.47
9	Fa_{30} + Kir_{70} + Ap +	Fa	29.94	0.00	0.00	63.32	1.96	0.52	4.20	0.00	99.94	1100	-10.3	-0.8	0.48
	Hd + Sulph	Kir	31.31	0.00	0.00	44.06	1.56	0.29	22.46	0.00	99.68	1050	-11.1	-0.9	0.45
		Hd	43.73	0.07	4.24	27.62	0.56	0.47	22.36	0.22	99.27				

Note: Fa_{40} + Kir_{60} are approximate modal contents of Fa and Kir in Fa-Kir intergrowths (original Ca-Fe olivine). Sulph = sulphides, other symbols see Table 2. Associations 6 and 7 are shown in Fig. 1 and 3B, respectively.

$10^{-10\text{-}10.3}$ and $10^{-10.8\text{-}11.1}$ bar at 1100 and 1050 °C, respectively, which is between 0.5 and 0.9 log units below the QFM buffer. The estimated silica activity ranged from 0.4 to 0.66.

Discussion

During long-term natural combustion of coal seams and bituminous matter in sedimentary rocks, temperature obtained are frequently high enough (900–1600 °C) to produce partial or total melting of the original rocks. The originated melts vary in composition from basic to acid ones (Venkatesh, 1952; Church *et al*., 1979; Bentor *et al*., 1981; Foit *et al*., 1987; Cosca *et al*., 1989; Kalugin *et al*., 1991). Basic ferrous paralavas which are comparable in chemical composition to Uralian parabasalts, are the most abundant of these melts. They are found in East Siberia, Russia (Yavorsky & Radugina, 1932); British Columbia, Canada (Church *et al*., 1979), Wyoming, USA (Foit *et al*., 1987; Cosca *et al*., 1989), and East Kazakhstan (Kalugin *et al*., 1991).

Fayalitic olivines are common minerals in some basic paralavas (Yavorsky & Radugina, 1932; Cosca *et al*., 1989; Kalugin *et al*., 1991). However, so far neither kirschsteinite nor solid solutions of the Fe_2SiO_4–$CaFeSiO_4$ series are found in natural pyrometamorphic rocks. Inasmuch as the Uralian parabasalts are similar in chemical composition to known basic paralavas, a possible reason for this fact is assumed to be the peculiarities of melt crystallisation conditions.

During natural subsurface combustion of coal seams, rapid cooling in paralavas may have been produced by circulation of cooler air along earlier cracks and suddenly opening fractures, as well as slumps of the roof rocks (Bustin & Mathews, 1982; Cosca *et al*., 1989). The cooler air intakes produce not only sharp temperature decrease, but also essential oxygen fugacity increase. This resulted in mass crystallisation of magnetite, magnesioferrite and/or hematite. These paralavas indicate oxidation states close to the QFM buffer or even approaching those of the hematite-magnetite buffer (Cosca & Peacor, 1987; Foit *et al*., 1987; Cosca *et al*., 1989). Their constituent silicates containing Fe^{2+} include augite, hedenbergite, Fe-rich olivine, Fe-cordierite and are present to an extent less than the ore phase contents (Yavorsky & Radugina, 1932; Kalugin *et al*., 1991). Among the silicates enriched in Fe^{3+}, unusual clinopyroxene (esseneite), melilite, and dorrite, were found in pyrometamorphic rocks from Wyoming (Cosca & Peacor, 1987; Foit *et al*., 1987; Cosca *et al*., 1989).

Fe-rich olivines in natural paralavas were the early crystallising phases, which grew under rapid cooling condi-

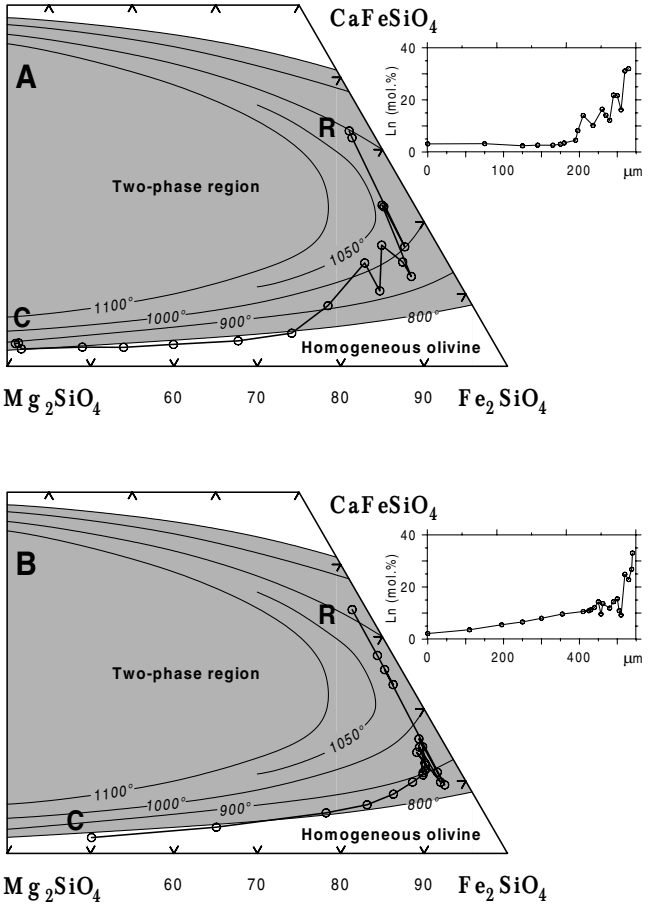

Fig. 6. Profiles of zoned Mg-Fe olivine grains rimmed by kirschsteinite-fayalite intergrowths, inserted in the Mg_2SiO_4-Fe_2SiO_4-Ca_2SiO_4 diagram. A – zoned Mg-Fe olivine (grain A in Table 4), B – zoned Mg-Fe olivine–calcian fayalite (grain B in Table 4). Isotherms of miscibility gap indicate calculated data according to Davidson & Mukhopadhyay (1984).

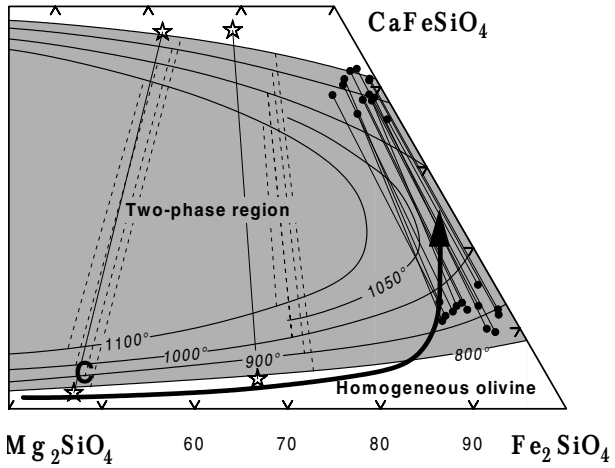

Fig. 7. Coexisting fayalite and kirschsteinite from intergrowths (solid circles) and possible evolution of the olivine composition during crystallisation of parabasalt (arrow). Stars are Mg-Fe-Ca olivines from meteorites (Prinz *et al.*, 1977; Mikouchi *et al.*, 1995). Coexisting phases are connected with solid tie lines. Isotherms of miscibility gap and dashed tie lines indicate data according to Davidson & Mukhopadhyay (1984).

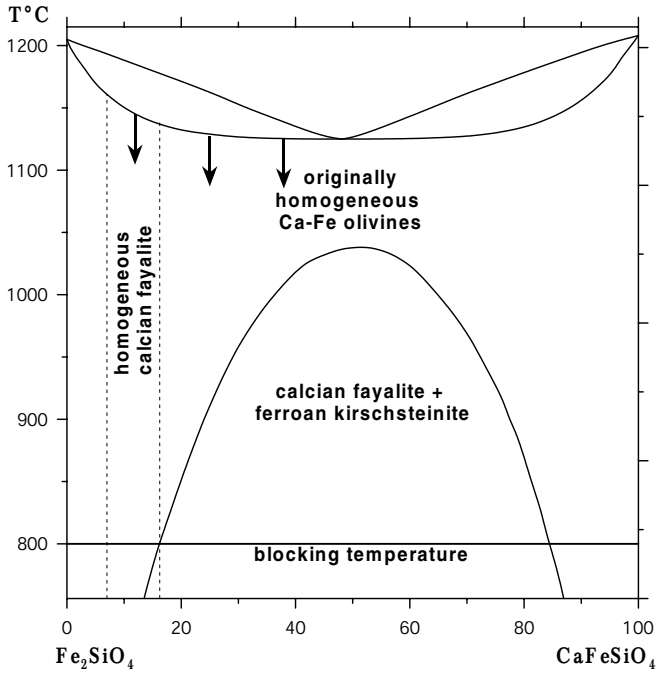

Fig. 8. Thermal history of the Ca-Fe olivines from the parabasalt in the Fe_2SiO_4-$CaFeSiO_4$ diagram. Field boundaries are according to Mukhopadhyay & Lindsley (1983). Blocking temperature of veined parabasalt was determined by compositions of the fayalite-kirschsteinite pairs (Fig. 7).

tions, as evidenced by quenching textures and by abundant features such as skeletal, hopper and spinifex crystals within the glass (Cosca *et al.*, 1989; Kalugin *et al.*, 1991). On the contrary, Ca-Fe olivines in the Uralian parabasalts do not display any quenching textures and are the late interstitial phases. Textural relationships of minerals in the veined parabasalt suggest that Ca-Fe olivine terminate an evolutionary series of minerals of this family: Mg-Fe olivine (Fo_{60-20}) → calcian fayalite → ferroan kirschsteinite. As distinct from the above-mentioned natural paralavas, man-induced melts in the Chelyabinsk spoil-heaps were cooling down rather slowly under a thick roof of heated overlying rocks. The duration of thermal action, from flame combustion (T = 1000–1200 °C) to cooling down to 150–300 °C is 15–20 years for the large spoil-heaps. Consequently, the cooling rate for the inner parts of the spoil-heaps can be estimated to be as 35–70 °C per year.

The appearance of Ca-Fe olivine is stipulated by the specific composition of the initial melt as well as by low oxygen fugacity, which is 2 log units below the QFM buffer, during the early stages of melt crystallisation. These conditions resulted in fractional crystallisation with a compositional trend showing Mg depletion and Fe^{2+} enrichment on cooling. This process is believed to be analogous to lunar ferrobasalt fractionation, investigated in detail by Brown *et al.* (1970) and Essene *et al.* (1970). During crystallisation of the early minerals (Al-spinel, anorthite, Mg-Fe olivine, augite) an initial melt was enriched in P, Mn, Fe, and Ti and depleted in Si and Al, with respect to the residue with high Ca content. This is confirmed by our data on compositions of the melt inclusions in the early minerals of parabasalts. The pro-

nounced zoning of olivines from parabasalts provides an additional support for the assumption that the liquid composition became enriched in Fe^{2+} during melt fractionation. At the final stage of crystallisation (T < 1150 °C) the interstices were filled with a low-silica melt enriched in CaO (15–17 wt. %) and FeO (22–41 wt. %) (Table 3). As the result of this crystallisation path, the later phases with high Fe and Ca contents (magnetite, fayalite, Ca-Fe olivines, kirschsteinite**,** hedenbergite) appeared. Besides the high concentrations of FeO and CaO, the low silica activity (a_{SiO2} = 0.4–0.6) is thought to be responsible for the unusually Ca-rich composition of primary Fe olivines.

During cooling of parabasalts (1030 °C ≤ T ≤ 800 °C), primary Ca-Fe olivines (8.5 ≤ CaO ≤ 20 wt. %) were subjected to exsolution with the formation of low-Ca (Fe_2SiO_4) and high-Ca ($CaFeSiO_4$) phases. Low oxygen fugacity and low silica activity played an essential role not only in the formation of Ca-Fe-olivine, but also in its following exsolution. Otherwise, hedenbergite and magnetite would exsolve from Ca-Fe olivine at higher f_{O2} (above the QFM buffer) and higher silica activity (Markl *et al.*, 2001).

Acknowledgments: The authors have benefited greatly from the comments of Yuri Dublyansky who helped to improve the manuscript. Constructive and thoughtful comments by D.H. Lindsley, E.J. Essene and C. Chopin have also greatly improved the early version of the manuscript. We also thank V. Lukyanov (Institute of Hydrodynamics, Novosibirsk, Russia) for BSE images acquisition. Financial support was given by the Russian Fund for Fundamental Research (N 98-05-65257 and 01-05-65060).

References

Andersen, D.J., Lindsley, D.H., Davidson, P.M. (1993): QUILF: a Pascal program to assess equilibria among Fe-Mg-Mn-Ti oxides, pyroxenes, olivine, and quartz. *Computers & Geosciences*, **19** (9), 1333–1350.

Anshits, A.G., Voskresenskaya, E.N., Kondratenko, E.V., Fomenko, E.V., Sokol, E.V. (1998): The study of composition of high temperature catalysts for oxidative conversion of methane. *Catalysis Today*, **42** (2), 197–203.

Ariskin, A.A., Frenkel, M.Ya., Barmina, G.S., Nielsen, R.L. (1993): COMAGMAT: a Fortran program to model magma differentiation processes. *Computers & Geosciences*, **19** (8), 1155–1170.

Bentor, Y.K., Kastner, M., Perlman, I., Yellin, Y. (1981): Combustion metamorphism of bituminous sediments and the formation of melts of granitic and sedimentary composition. *Geochim. Cosmochim. Acta*, **45**, 2229–2255.

Brown, G.M., Emeleus, C.H., Holland, J.G., Phillips, R. (1970): Mineralogical, chemical and petrological features of Apollo 11 rocks and their relationship to igneous processes. *in* "Proceedings of the Apollo 11 lunar science conference". V. 1 "Mineralogy and petrology", A.A. Levinson, ed. Pergamon Press, New York, 195–219.

Bustin, R.M. & Mathews, W.H. (1982): *In situ* gasification of coal, a natural example: History, petrology, and mechanics of combustion. *Can. J. Earth. Sci.*, **19**, 514–523.

Chalapathi, R.N.V., Reed, S.J.B., Pyle, D.M., Beattie, P.D. (1996): Larnitic kirschsteinite from the Kotakonda kimberlite, Andra Pradesh, India. *Mineral. Mag.*, **60**, 513–516.

Chesnokov, B.V. & Shcherbakova, E.P. (1991): The mineralogy of burned heaps in the Chelyabinsk coal basin. Publ. H. Nauka, Moscow, 152 p. (in Russian).

Church, B.N., Matheson, A., Hora, Z.D. (1979): Combustion metamorphism in the Hat Creek area, British Columbia. *Can. J. Earth Sci.*, **16**, 1882–1887.

Cosca, M.A. & Peacor, D.R. (1987): Chemistry and structure of esseneite, ($CaFe^{3+}AlSiO_6$), a new pyroxene produced by pyrometamorphism. *Am. Mineral.*, **72**, 148–156.

Cosca, M.A., Essene, E.J., Geissman, J.W., Simmons, W.B., Coates, D.A. (1989): Pyrometamorphic rocks associated with naturally burned coal beds, Powder River Basin, Wyoming. *Am. Mineral.*, **74,** 85–100.

Davidson, P.M. & Mukhopadhyay, D.K. (1984): Ca-Fe-Mg olivines: Phase relations and a solution model. *Contrib. Mineral. Petrol.*, **86**, 256–263.

Deer, W.A., Howie, R.A., Zussman, J. (1982): Rock-forming minerals. – Orthosilicates. Vol. 1A. Longman, London and New York, 919 p.

Dodd, R.T. (1971): Calc-aluminous inset in olivine of the Sharps chondrite. *Mineral. Mag.*, **38**, 451–458.

Essene, E.J., Ringwood, A.E., Ware, N.G. (1970): Petrology of the lunar rocks from Apollo 11 landing site. *in* "Proceedings of the Apollo 11 lunar science conference". V. 1 "Mineralogy and petrology", A.A. Levinson, ed. Pergamon Press, New York, 385–397.

Fermor, L.L. (1918): Preliminary note on the burning of coal seams at the outcrop. *Trans. Min. Geol. Inst. India*, **12**, 50–63.

Foit, F.F., Hooper, R.L., Rosenberg, P.E. (1987): An unusual pyroxene, melilite, and iron oxide mineral assemblage in a coal-fire buchite from Buffalo, Wyoming. *Am. Mineral.*, **72**, 137–147.

Folco, L. & Mellini, M. (1997): Crystal chemistry of meteoritic kirschsteinite. *Eur. J. Mineral.*, **9**, 969–973.

Gustafson, W.I. (1972): The stability of andradite, hedenbergite and related minerals in the system Ca-Fe-Si-O-H. *J. Petrol.*, **15**, 455–496.

Kahn, J.S. & Smith, D.K. (1966): Mineralogical investigations in the debris of the Gnome event near Carlsbad, New Mexico. *Am. Mineral.*, **51**, 1192–1199.

Kalugin, I.A., Tretyakov, G.A., Bobrov, V.A. (1991): Iron ore basalts in burned rocks of Eastern Kazakhstan. Publ. H. Nauka, Novosibirsk, 80 p. (in Russian).

Kilinc, A., Carmichael, I.S.E., Rivers, M.L., Sack, R.O. (1983): The ferric-ferrous ratio of natural silicate liquids equilibrated in air. *Contrib. Mineral. Petrol.*, **83**, 136–140.

Krot, A.N., Petaev, M.I., Meibom, A., Keil, K. (2000): In situ growth of Ca-rich rims around Allende dark inclusions. *Geochem. Int.*, **38**, 351–368.

Longhi, J. (1999): Phase equilibrium constraints on angrite petrogenesis. *Geochim. Cosmochim. Acta*, **63**, 573–585.

Markl, G., Marks, M., Wirth, R. (2001): The influence of T, a_{SiO2}, and f_{O2} on exsolution textures in Fe-Mg olivine: An example from augite syenites of the Ilímaussaq Intrusion, South Greenland. *Am. Mineral.*, **86**, 36–46.

McKay, G.A., Miyamoto, M., Mikouchi, T., Ogawa, T. (1998): The cooling history of the Lewis Cliff 86010 angrite as inferred from kirschsteinite lamellae in olivine. *Meteor. Planet. Sci.*, **33**, 977–983.

Mikouchi, T., Takeda, H., Miyamoto, M., Ohsumi, K., McKay, G.A. (1995): Exsolution lamellae of kirschsteinite in magnesium-iron olivine from an angrite meteorite. *Am. Mineral.*, **80**, 585–592.

Mittlefehldt, D.W. & Lindstrom, M.M. (1990): Geochemistry and genesis of the angrites. *Geochim. Cosmochim. Acta*, **54**, 3209–3218.

Mukhopadhyay, D. K. & Lindsley, D. H. (1983): Phase relations in the join kirschsteinite ($CaFeSiO_4$) – fayalite (Fe_2SiO_4). *Am. Mineral.*, **68**, 1089–1094.

Nickel, E.H. (1995): Mineral names applied to synthetic substances. *Can. Mineral.*, **33**, 1335.

Nickel, E.H. & Grice, J.D. (1998): The IMA commission on new minerals and mineral names: procedures and guidelines on mineral nomenclature, 1998. *Can. Mineral.*, **36**, 913–926.

Oleinikov, A.A. (1995): Kirschsteinite is the probable product of symplectitic exsolution of early magmatic calcium-containing hyalosiderite. *Dokl. Russ. Acad. Sci.*, **342** (1), 80–81.

Prinz, M., Keil, K., Hlava, P.F. Berkley, J.L., Gomes, C.B., Curvello, W.S. (1977): Studies of Brazilian meteorites. III. Origin and history of the Angra dos Reis achondrite. *Earth Planet. Sci. Lett.*, **35**, 317–330.

Sahama, Th.G. & Hytönen, K. (1957): Kirschsteinite, a natural analogue to synthetic iron monticellite from Belgian Congo. *Mineral. Mag.*, **31** (239), 698–699.

Sharygin, V.V., Kalugin, V.M., Nigmatulina, E.N., Sokol, E.V. (1999a): Silicate-melt inclusions in minerals of technogeneous parabasalts, Chelyabinsk brown coal basin, South Urals, Russia. *Terra Nostra*, N 6, 271–274.

Sharygin, V.V., Sokol, E.V., Nigmatulina, E.N., Lepezin, G.G., Kalugin, V.M., Frenkel, A.E. (1999b): Mineralogy and petrography of technogene parabasalts of the Chelyabinsk coal basin. *Russ. Geol. Geophys.*, **40** (6), 879–889.

Simkin, T. & Smith, J.V. (1970): Minor element distribution in olivine. *J. Geol.*, **78**, 304–325.

Sokol, E.V., Volkova, N.I., Lepezin, G.G. (1998): Mineralogy of pyrometamophic rocks associated with naturally burned coal-bearing spoil-heaps of the Chelyabinsk coal basin, Russia. *Eur. J. Mineral.*, **10**, 1003–1014.

Sokol, E.V., Kalugin, V.M., Sharygin, V.V., Nigmatulina, E.N. (2001): Origin of ferrous paralavas. *in* "Mineralogy of technogenesis – 2001", S.S. Potapov, ed. Publ. I Min Ur. B. RAS, Miass, 148–170 (in Russian).

Sokol, E.V., Nigmatulina, E.N., Volkova, N.I. (2002): Fluorine mineralisation from burning coal spoil-heaps in the Russian Urals. *Mineral. Petrol.*, **75** (in press).

Stormer, J.C. (1973): Calcium zoning in olivine and its relationship to silica activity and pressure. *Geochim. Cosmochim. Acta*, **37**, 1815–1821.

Tolstykh, N.D., Krivenko, A.P., Elisafenko, V.N., Ponamarchuk, V.A. (1991): Mineralogy of apatite-bearing carbonatites from the Kuznetsk Alatau. *Sov. Geol. Geophys.*, **32**, 41–48.

Venkatesh, V. (1952): Development and growth of cordierite in paralavas. *Am. Mineral.*, **37**, 831–848.

Wyderko, M. & Mazanek, E. (1968): The mineralogical characteristics of calcium-iron olivines. *Mineral. Mag.*, **36**, 955–961.

Yavorsky, V.I. & Radugina, L.V. (1932): Coal-fire combustion and attendant events in Kuznetsky basin. *Mining Journal*, **10**, 55–59 (in Russian).

Received 22 May 2000
Modified version received 17 January 2002
Accepted 4 February 2002